Clim Dyn
DOI 10.1007/s00382-010-0804-4

Spatiotemporal drought variability in northwestern Africa over the last nine centuries

Ramzi Touchan · Kevin J. Anchukaitis · David M. Meko · Mohamed Sabir · Said Attalah · Ali Aloui

Received: 9 December 2009 / Accepted: 22 March 2010

Abstract Changes in precipitation patterns and the frequency and duration of drought are likely to be the feature of anthropogenic climate change that will have the most direct and most immediate consequences for human populations. The latest generation of state-of-the-art climate models project future widespread drying in the subtropics. Here, we reconstruct spatially-complete gridded Palmer drought severity index values back to A.D. 1179 over Morocco, Algeria, and Tunisia. The reconstructions provide long-term context for northwest African hydroclimatology, revealing large-scale regional droughts prior to the sixteenth century, as well as more heterogeneous patterns in sixteenth, eighteenth, and twentieth century. Over the most recent decades a shift toward dry conditions over the region is observed, which is consistent with general circulation model projections of greenhouse gas forced enhanced regional subtropical drought.

Keywords Tree-ring · Drought · Climate field reconstruction · Mediterranean · Northwestern Africa

1 Introduction

Society faces many challenges, few of them more complex than the need to conserve natural resources while providing the benefits of economic development to all sectors of the population. This challenge is particularly severe in arid and semi-arid regions, where the resource limitations come not merely from a shortage of water but from the high variability of precipitation in space and time. The critical balance of water in arid ecosystems is readily upset by the resource needs of dense human populations. Dry area covers one-third of the land surface of the earth; more than half of that area is home to 630 million people, and the remainder is so arid and unproductive that it cannot readily support human life (Brooks et al. 1991).

Various parts of North Africa have suffered devastating drought in the last 30 years (e.g. Nicholson and Wigley 1984; Chbouki 1992; Swearingen 1992; Hoerling and Kumar 2003). Drought impacts an economic and social structure already reeling from other serious problems. For example, Moroccan droughts between 1980 and 1985 caused food-shortages and violent civil unrest and drove Morocco's foreign debt to 80% of its gross national product (Swearingen 1992). Also during this early 1980's drought, river flow in Morocco decreased 50–90% from respective long-term mean flows (Chbouki 1992) and many natural lakes dried up completely (Belkheiri et al. 1987). More

Electronic supplementary material The online version of this article (doi:10.1007/s00382-010-0804-4) contains supplementary material, which is available to authorized users.

R. Touchan (✉) · D. M. Meko
Laboratory of Tree Ring Research, The University of Arizona, 105 W. Stadium, Tucson, AZ 85721-0058, USA
e-mail: rtouchan@ltrr.arizona.edu

K. J. Anchukaitis
Lamont Doherty Earth Observatory, Columbia University, 61 Route 9W, Palisades, NY 10964, USA

M. Sabir
National School of Forest Engineering, Sale, Morocco

S. Attalah
Department of Agronomy, University of Ourgla, 30100 Ouargla, Algeria

A. Aloui
Institute of Sylvo-pastoral of Tabarka, 8110 Tabarka, Tunisia

Published online: 13 April 2010

recently, the 1999–2002 droughts in North Africa appear by some metrics to perhaps be the worst since at least the middle of the fifteenth century (Touchan et al. 2008a). Recent drought in the region began in 1999, apparently part of a widespread pattern of midlatitude drying in the Northern Hemisphere (Hoerling and Kumar 2003). Increasingly dry subtropical conditions are one predicted consequence of anthropogenic climate change (Held and Soden 2006; Seager et al. 2007a; Chou et al. 2009). Future efficient use of limited water resources will require better and more effective planning processes to implement long-term management actions and other intervention strategies. Effective planning is currently constrained in part by the limitations of instrumental climate data: precipitation, temperature, and streamflow records generally cover only slightly more than 70 years in much of North Africa. These records are not long enough to determine the characteristic time scale and forcing of regional climate variability over several centuries, nor to identify whether the recent pattern of drought could be part of an 'imminent' change toward drier conditions in the region (c.f. Seager et al. 2007a).

Instrumental records can be extended back several centuries with proxy data. The resulting records can provide estimates of the past frequency and severity of climatic anomalies, and these in turn may be used to help anticipate the probability of such events in the future. Long time series of tree-ring growth are one of the best sources of proxy data for reconstructing past records of precipitation, streamflow, and drought on interannual to centennial time scales during the late Holocene. Tree-ring records are annually resolved, well-replicated, and can be calibrated and validated against the instrumental record. Morocco has a rich history of dendroclimatic research going back nearly 40 years (e.g Munaut et al. 1979; Berger et al. 1979; Till 1987; Till and Guiot 1990; Chbouki 1992; Chbouki et al. 1995; Glueck and Stockton 2001; Esper et al. 2007). Elsewhere in North Africa dendroclimatic studies are rare. Earlier studies in Algeria (Messaoudene 1989; Messaoudene and Tessier 1997; Safar et al. 1992) and Tunisia (Serre-Bachet 1969; Aloui 1982; Aloui and Serre-Bachet 1987; Tessier et al. 1994) were restricted to analysis of the relationship between annual tree-growth and climate. More recent studies yielded the first dendroclimatic reconstructions for Algeria and Tunisia (Touchan et al. 2008a, b), but focused on a large-scale mean regional tree-ring series.

In this paper we give results of the first large-scale systematic dendroclimatic sampling campaign across western North Africa. We introduce the full new tree-ring network, apply it to a climate-field reconstruction of drought, and analyze temporal and spatial features of the reconstruction. We then use the reconstruction to place recent drought in the context of long-term natural variability and expected future climate change.

2 Regional geography and climate

Our investigation focuses on long-term climate variability in the Mediterranean borderlands of northwestern Africa—Morocco, Algeria and Tunisia. The region has a predominantly Mediterranean climate, characterized by hot, dry summers and mild, wetter winters (Critchfield 1983). Mountains separate the extremely arid desert areas to the south from the somewhat more temperate northern areas dominated by moist Mediterranean and Atlantic winds, and strongly influence the distribution of precipitation and the extent of the influence of various climatic phenomena (Trewartha 1981). Interannual variability in the amount, intensity and spatial distribution of precipitation can be substantial throughout North Africa (Critchfield 1983). While October-April is the most prevalent wet season across the region, seasonal rains may be absent, or may begin as late as February or March. In Tunisia, the rainy season is typically December-March, with secondary wet periods in the spring and fall. Extensive floods from high intensity storms over a short period of time are common, as are extended periods of drought.

Regional climate variability in northwestern Africa is teleconnected to hemispheric-scale circulation patterns and oceanic influences (Atlantic Ocean and Mediterranean Sea), as well as the continental influences of Europe and the Saharan Desert (Trewartha 1981). Movement and development of winter cyclonic storms systems in the Mediterranean Basin are linked closely to shifts in positions of the Icelandic Low and Azores High, and resulting changes in upper level steering winds and polar-air intrusions (Trewartha 1981). The North Atlantic oscillation (NAO) is negatively correlated with winter (DJF) precipitation in Morocco, but correlation weakens toward the south and east (Lamb et al. 1997; Knippertz et al. 2003a). Indeed the spatial pattern of correlations of NAO across northwestern Africa is sensitive to the particular definition of NAO (Knippertz et al. 2003a). Increasing Mediterranean-sea influence on precipitation delivery toward the east is reflected both by such correlation patterns and by changes in circulation weather types associated with precipitation (Knippertz et al. 2003a).

3 Materials and methods

3.1 Chronology development

Our field collection targeted species *Cedrus atlantica*, *Pinus halepensis*, *Pinus pinaster*, *Abies marocan*, *Pinus nigra*, *Quercus afares*, and *Quercus canariensis*. Previous research has established that these species share a high degree of common variation that is strongly driven by

climate (Glueck and Stockton 2001; Chbouki et al. 1995; Esper et al. 2007; Touchan et al. 2008a, b). We developed new chronologies and enhanced (increased sample size) and extended existing chronologies. Increment cores were collected at 39 sites in Morocco, Algeria, and Tunisia, with additional full cross sections taken from selected stumps of cedar, oak, and pine when available (Figs. 1, 2; Table 1). Samples were fine-sanded and crossdated following standard dendrochronological techniques (Stokes and Smiley 1968; Swetnam 1985). The width of each annual ring on the cores and cross-sections was measured to the nearest 0.01 mm. Visual and graphical crossdating was confirmed using statistical pattern matching (Holmes 1983).

A uniform and systematic procedure was applied in chronology development. Each series of tree-ring width measurements was fit with a cubic smoothing spline with a 50% frequency response at 67% of the series length to remove non-climatic trends due to age, size, and the effects of stand dynamics (Cook and Briffa 1990). The detrended series were then prewhitened with low-order autoregressive models to remove persistence not related to climatic variations. The individual indices were combined into a single master chronology for each combination of site and species using a bi-weight robust estimate of the mean (Cook 1985). The adequacy of sample replication was judged by the expressed population signal (EPS), computed from pooled interseries correlations and the time-varying sample size (Wigley et al. 1984).

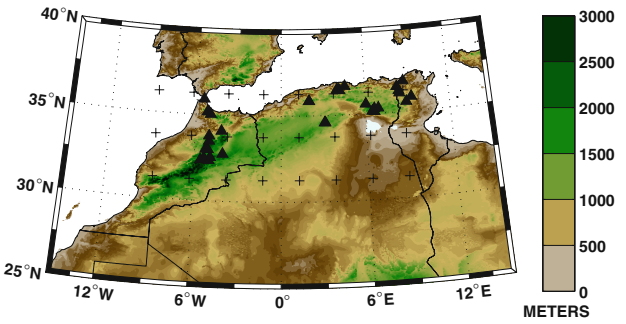

Fig. 1 The location of the tree ring chronology sites used in this study are indicated by the *triangles*. The target climate PDSI grid points (Dai et al. 2004) are indicated by *crosses*. Digital terrain elevation from the ETOPO2 dataset. Areas below sea level can be observed at Shatt al Gharsah in Tunisia and the Chott Melrhir Depression in Algeria

3.2 Climate field reconstruction

We use a point-to-point multiple nested regression approach (Cook et al. 1999, 2004) to reconstruct May–August average Palmer drought severity index (PDSI) at each of 24 grid points covering the region. Summer-average PDSI integrates precipitation and temperature during much of the year, including the winter Mediterranean wet season, and

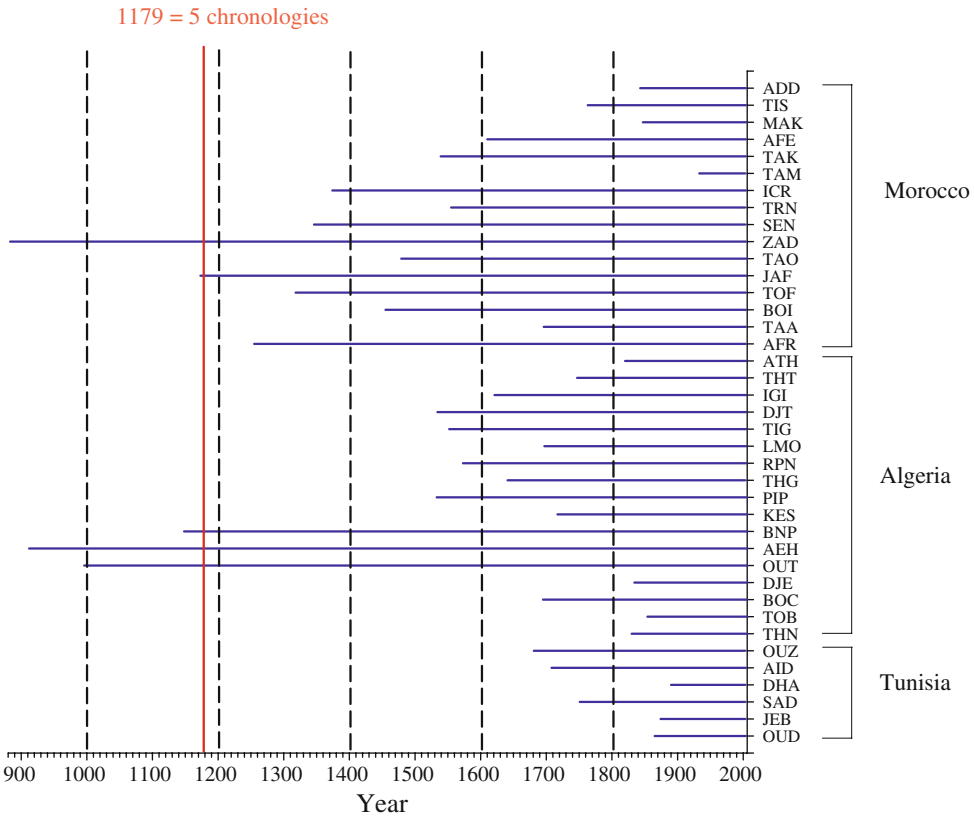

Fig. 2 Graphical representation of the span of each chronology developed from Morocco, Algeria, and Tunisia. The A.D. 1179 cutoff used here is demarcated where the regional sample depth falls below five individual sites. Small differences (<5 years) in the length of the full 'standard' chronology length (Table 2) and the 'residual' chronologies used in this study and shown in this figure arise from the process of autoregressive modeling

Table 1 Site information for North Africa

Site name	Code	Country	Species	Elevation (m)	Latitude	Longitude	Time span	# Years	# Trees	# Cores
Addeldal	ADD	Morocco	PIPI	850–950	35°54′N	05°28′W	1843–2004	162	20	39
Tissoukaa	TIS		ABMA	1750–1800	35°11′N	05°12′W	1763–2004	242	20	37
Madissoukaa	MAK		PINI	1300–1400	35°10′N	05°08′W	1847–2005	159	15	28
Affechtal	AFE		CEAT	1750–1850	35°02′N	04°59′W	1610–2004	394	20	40
Tazzeka	TAK		CEAT	1800–1950	34°05′N	04°11′W	1539–2004	466	23	46
Tamjot	TAM		PIPI	1450–1550	33°52′N	04°W	1933–2004	71	11	20
Ich Ramouz	ICR		CEAT	1800–1850	33°47′N	05°02′W	1374–2004	631	23	45
Tizi u Treten	TRN		CEAT	1856–1921	33°28′N	05°01′W	1555–2003	449	23	46
Senoual	SEN		CEAT	1976–2144	33°00′N	05°15′W	1346–2003	657	25	50
Col Du Zad	ZAD		CEAT	2106–2300	32°59′N	05°04′W	883–2004	1122	72	126
Taourirt	TAO		CEAT	1850–1900	32°45′N	04°03′W	1479–2004	526	21	43
Jafaar	JAF		CEAT	2053–2183	32°32′N	04°54′W	1173–2004	816	24	38
Tounfite	TOF		CEAT	2100–2200	32°28′N	05°20′W	1318–2004	687	21	40
Bouizourane	BOI		CEAT	2150–2200	32°27′N	05°19′W	1455–2004	550	21	41
Tadlounte	TAA		CEAT	1858–1988	32°22′N	05°34′W	1696–2004	309	20	49
Afrasko	AFR		CEAT	2400–2500	32°21′N	05°00′W	1256–2004	749	18	34
Athmane	ATH	Algeria	QUAF	1042–1117	36°40′N	04°34′E	1820–2005	186	15	22
Thamguig-uelt	THT		CEAT	1500–1600	36°28′N	04°01′E	1747–2005	259	20	40
Ignilinuel	IGI		CEAT	1422–1463	36°28′N	04°00′E	1621–2005	385	20	41
Djamatighr-ifine	DJT		CEAT	1451–1494	36°27′N	04°06′E	1534–2005	472	21	46
Tigounetine	TIG		CEAT	1690–1743	36°27′N	04°06′E	1552–2006	455	20	40
Leid Mohamad Ouali	LMO		CEAT	1500–1535	36°27′N	04°06′E	1697–2005	309	19	33
Pinus Nigra Reserve	RPN		PINI	1520–1596	36°27′N	04°06′E	1573–2005	433	20	37
Thala Gaidawane	THG		CEAT	1296–1450	36°26′N	04°12′E	1641–2005	365	20	40
Pipiniere Parasol	PIP		CEAT	1431–1472	35°51′N	01°59′E	1533–2006	474	19	36
Kef-Sahchine	KES		CEAT	1543–1567	35°51′N	02°00′E	1717–2006	290	20	38
Bordjem National Park	BNP		CEAT	1841–1882	35°35′N	06°02′E	1148–2006	859	27	51
Ain El Halfa	AEH		CEAT	1734–1776	35°19′N	06°54′E	912–2006	387	23	42
Ouad Tider	OUT		CEAT	2030–2146	35°18′N	06°37′E	996–2006	1095	32	53
Djeniene	DJE		PIHA	1134–1226	35°09′N	06°28′E	1834–2006	173	19	38
Bout-Chaout	BOC		PIHA	1250–1296	35°07′N	06°37′E	1695–2006	312	22	35
Tobji	TOB		PIHA	1323–1456	34°36′N	03°07′E	1854–2006	153	20	38
Theniet	THN		PIHA	1380–1405	34°36′N	03°05′E	1830–2006	177	20	40
Oued Zen	OUZ	Tunisia	QUCA	382–730	36°47′N	08°47′E	1681–2003	323	16	16
Ain Dhalia	AID		QUCA	671–750	36°29′N	08°18′E	1708–2003	296	17	17
Dahllia	DHA		PIHA	919–981	36°14′N	08°26′E	1890–2003	114	11	22
Sadine	SAD		PIHA	383–464	36°06′N	08°29′E	1751–2003	253	24	47
Jebnoun	JEB		PIHA	792–810	35°51′N	09°18′E	1874–2003	130	15	30
Oum Djedour	OUD		PIHA	1000–1100	35°35′N	08°56′E	1865–2004	140	20	28

Species codes: PIPI *Pinus pinaster*, ABMA *Abies marocan*, PINI *Pinus nigra*, CEAT *Cedrus atlantica*, QUAF *Quercus afares*, PIHA *Pinus halepensis*, QUCA *Quercus canariensis*. The time span for each site listed in the table reflects the full length of the (standard) chronology. The process of prewhitening the series with low order autoregressive models to develop the 'residual' chronology in some cases reduces the total length by several (<5) years. Figure 2 reflects the time span of the residual chronologies used in the reconstruction

therefore provides a uniform predictand target over the full spatial domain that reflects the moisture available to trees during the growth season (Cook et al. 1999). Such a target has been found elsewhere advantageous in that it is relatively insensitive to differences in the precise monthly or seasonal tree-ring response to precipitation across a broad multi-species tree-ring network (Cook et al. 1999, 2004) and is highly correlated with tree growth in semiarid environments (Kempes et al. 2007). A PDSI value of −1 is 'mild' drought, a value of −3 is 'severe drought', and the metric is

designed to be comparable across climate regimes (Palmer 1965). May through August was identified from previous analysis of the climate signal to be consistent with the most highly correlated seasonal PDSI span for the tree-ring chronologies over the full spatial domain (Esper et al. 2007; Touchan et al. 2008a). This specific period was initially established in Touchan et al. (2008a). The target field is from the global gridded PDSI dataset developed by Dai et al. (2004) and has a spatial resolution of 2.5°. This grid is shown in Fig. 1. The point-to-point methodology seeks to reconstruct the past climate variability at each target grid location separately, with the available subset of all tree-ring predictors determined by their distance from the grid point centroid. In this study we used a fixed search radius of 500 km, which is comparable to reconstructions using point-to-point regression methodology employing a 450 km radius in the more densely-sampled regions of North America (Cook et al. 1999, 2004). This search radius is also consistent with the spatial decorrelation pattern of the instrumental data (Fig. 3) and furthermore allows each of the 24 grid points to be reconstructed for at least a portion of the full time domain, and over the full time span for the majority of the field. With the exception of the central southern part of the target field, where few tree ring chronologies now exist, the PDSI reconstruction is otherwise spatially and temporally complete. We note that the orographic features of the region (Fig. 1) can result in a search radius that permits a pool of

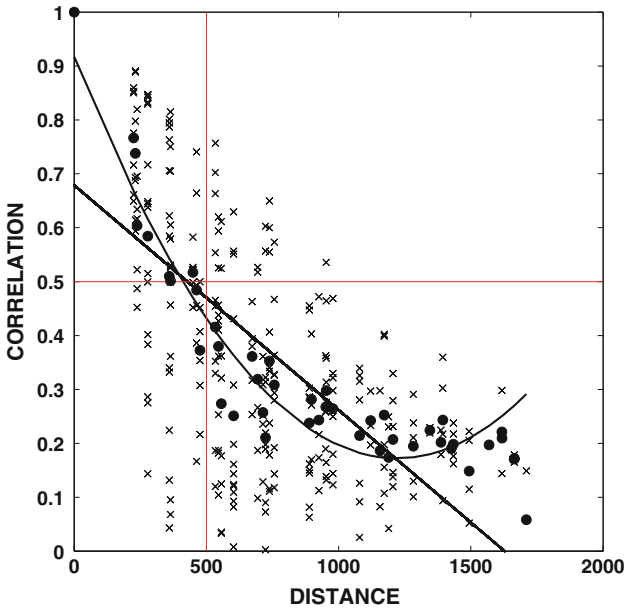

Fig. 3 Instrumental PDSI grid point-to-point correlation as a function of distance between grid points, indicated by *crosses*. *Thick black lines* show the linear and polynomial least squares fits to the data. *Filled circles* are the biweight robust mean correlation at each distance. The *red lines* indicate $r = 0.50$ (*horizontal*) and 500 km (*vertical*). The range of correlation values for a given distance is largely due to orographic and topographic features of the region

available predictors that come from regions with potentially different climate regimes than the target grid cell itself. This largely explains the range of distance-mediated correlations evident in Fig. 3; however, distal chronologies from regions without covarying climate variability are unlikely to result in additional reconstruction skill and therefore will not influence the final reconstruction.

We used the individual master chronologies as the potential predictors to develop a set of nested multivariate stepwise regression models (Meko 1997; Cook et al. 2002; Wilson et al. 2006). In this procedure, an estimate of past drought values at a grid point is first calculated from the stepwise regression model for the period covered by all the individual site chronologies. Additional statistical models are then sequentially developed for progressively longer periods back in time, with their span corresponding to the changes in the availability of the underlying predictor tree-ring series. Here, we have used every change in sample depth in time to objectively identify the earliest date of each subsequent nest. The individual reconstructions in this manner are scaled to have the standard deviation of the best replicated, most recent nest, and joined into a single long reconstruction such that each time period is represented by the corresponding regression model with the greatest available data. Entry into the multivariate linear stepwise model was based on the adjusted R^2 statistic.

The skill of the reconstruction was assessed using the adjusted calibration R^2, the root mean square error (RMSE) of the calibration and validation periods, and the reduction of error and coefficient of efficiency statistic (Cook et al. 1994; Wilson et al. 2006). This procedure permits the skill of the drought reconstruction to be estimated as a function of the changing set of available predictor data (Meko 1997). The calibration–validation procedure was performed 3 times—with a late calibration (1969–2003) and early validation period (1931–1968), an early calibration period and late validation period, and then using the full period for calibration and performing validation using an additional leave-one-out validation jackknife procedure. The R^2 and RMSE statistics provide a good measure of the accuracy of the high-frequency component of the reconstruction, while the RE and CE further evaluate the skill of the reconstruction beyond climatology (in this case, represented by the calibration or validation period mean, respectively). RE in particular is useful for verifying that the reconstruction can accurately reproduce any changes between the calibration and validation period mean (Cook et al. 1994; Ammann and Wahl 2007).

3.3 Time series analysis

We analyzed reconstructed PDSI series in the time domain by low-pass filtering and in the frequency domain by cross-

spectral analysis and wavelet analysis. When isolating decadal-scale variability, time series were smoothed with a Butterworth filter with series padding optimally selected to minimize the mean squared error and to avoid misleading behavior at the end of the series (Mann 2004). Covariation of pairs of series over their full length of overlap was summarized in the frequency domain by smoothed-periodogram cross-spectral analysis (Bloomfield 2000). Quantities examined were the variance spectra, coherency spectrum and phase spectrum. Processing steps included subtraction of sample means, tapering of each end (5%) with a split-cosine-bell filter, padding with zeros to length equal to the next power of 2 above the sample-size, and computation of the discrete Fourier transform (DFT). Periodograms and cross-periodograms were then computed from the DFTs and developed as estimates of spectra and cross-spectra by smoothing with a sequence of Daniell filters. Filters were selected such that the bandwidth of spectral estimates was approximately 0.05 cycles/year. Following Bloomfield (2000), coherency and phase spectra were then computed from the various spectral quantities and plotted with confidence bands to summarize covariation of time series. Confidence bands were computed as in Meko and Woodhouse (2005). Phase is poorly determined when coherence is low (Bloomfield 2000). Accordingly, following Bloomfield (2000), confidence intervals on the coherency and phase are plotted only over those frequency intervals for which the squared coherency passes a simplified test for 95% significance. The time evolution of simultaneous or asynchronous regional drought was summarized by a wavelet coherency spectrum (Maraun and Kurths 2004).

Simple Pearson correlations were used to the gauge strength of the relationship of selected reconstructed PDSI series with the North Atlantic oscillation (NAO). The NAO index for this analysis is the winter-average (DJFM) difference of normalized sea level pressure (SLP) between Lisbon, Portugal and Stykkisholmur/Reykjavik, Iceland. This index, 1864–2009, was downloaded from the website of the Climate Analysis Section of NCAR (http://www.cgd.ucar.edu/cas/jhurrell/indices.html). Spatial correlation fields were also calculated with gridded sea surface temperature anomalies (SST; Kaplan et al. 1998).

3.4 General circulation model simulations

In order to compare our drought reconstruction with possible patterns of forced and stochastic climate variability, we used precipitation and temperature data from the World Climate Research Programme's (WCRP's) Coupled Model Intercomparison Project phase 3 (CMIP3) multi-model dataset (Meehl et al. 2007) to calculate the model-simulated northwestern African summer PDSI. For the forced response, we used a 68 member ensemble from 23 coupled general circulation models from the twentieth century simulation ('20c3m'). For our control, we used the last 150 years from each simulation of the preindustrial control experiment ('picntrl', with no transient forcing) from a 26 member ensemble including 20 individual climate models. We then calculated a simulated PDSI for each ensemble member similar to Dai et al. (2004), although using Palmer's original available water capacity for the two level soil model (Palmer 1965; Touchan et al. 2008a). CMIP3 models have horizontal (latitude $\times$ longitude) resolutions that range from $\sim 1.1^\circ \times 1.1^\circ$ to $4^\circ \times 5^\circ$. PDSI values for all model grid points corresponding to our target instrumental field were averaged in space to create a simulation mean time series, then all standardized [0, 1] ensemble member series for each scenario were averaged to create a scenario mean time series that could be compared to our reconstruction regional mean.

4 Results and discussion

4.1 Tree ring chronologies

We developed a total of 39 ring-width chronologies from Morocco, Algeria, and Tunisia (Fig. 1). We removed one Moroccan chronology, Tamjot (TAM), from the analysis because it was short (spanning only A.D. 1933–2002). Statistical analyses of each chronology are summarized in Table 2. The mean correlation among individual radii at each site represents the strength of their common signal and ranges from 0.32 to 0.82. The highest interseries correlation is for Djeniene (Algeria) and the lowest is for the chronologies developed from Tissouka and Madissouka in Morocco and Thala Gaidawane in Algeria. The mean sample segment length (MSSL) of the 39 chronologies ranges from 55 to 525 years. Half of the chronologies have MSSL greater than 200 years and many have samples exceeding 300 years. Our longest tree ring chronology, from Col de Zad in Morocco, extends back to A.D. 883, and has an EPS statistic greater than 0.85 after A.D. 918 (Table 2). Ouad Tider in Algeria extends back to A.D. 912 and meets the same EPS threshold after the middle of the eleventh century. Although several chronologies span the entire last millennium, chronology statistics and regional sample depth lead us to identify the period from A.D. 1179 onward covered by at least 5 prewhitened chronologies as the most reliable, and we focus our interpretation on this epoch.

4.2 Reconstruction skill

Reconstruction skill at each grid point was assessed individually for each nest, and the full calibration and

validation statistics for each are available as Supplemental Materials. In general, the reconstructed variance and skill is highest in the western and eastern part of the target domain, irrespective of the calibration and validation period (Figs. 4, 5, 6). Variance accounted for by the reconstruction in Morocco, eastern Algeria, and Tunisia exceeds 40% in the best replicated nests in the most recent centuries, and is still approximately 20% in these regions back through the earlier part of the millennium, when only a total of 5 chronologies are available in the western and eastern regions. Over the eastern and western poles of the domain, up to ~80% of the calibration period variance is

Table 2 Chronology summary statistics

Site code	Country	MSSL[a]	std[b]	SK[c]	KU[d]	EPS > 0.85[e]	Common interval	MCAR[f]	% EV PC1[g]
ADD	Morocco	99	0.13	−0.15	1.38	1914	1944–2001	0.36	38
TIS		166	0.13	0.04	−0.12	1839	1870–2003	0.32	35
MAK		93	0.12	−0.01	0.01	1942	1933–2001	0.32	36
AFE		236	0.14	−0.12	0.01	1657	1772–2002	0.44	46
TAK		220	0.21	−0.40	1.47	1775	1868–2004	0.43	45
TAM		55	0.21	−0.71	2.85	1962	1966–2003	0.40	46
ICR		393	0.19	−0.86	2.15	1416	1573–1972	0.47	51
TRN		227	0.22	0.33	6.61	1631	1842–2000	0.49	51
SEN		345	0.20	−0.76	1.80	1405	1756–1991	0.45	48
ZAD		471	0.25	−0.48	1.23	918	1499–1840	0.55	56
TAO		245	0.26	−1.16	2.06	1682	1793–1999	0.48	51
JAF		327	0.33	−0.33	0.22	1262	1698–1965	0.60	62
TOF		296	0.32	−0.24	0.28	1369	1654–1965	0.65	68
BOI		303	0.35	−0.19	0.08	1452	1682–1998	0.65	67
TAA		203	0.26	−0.83	2.30	1726	1801–1980	0.61	63
AFR		525	0.40	0.62	0.02	1321	1549–1980	0.71	72
ATH	Algeria	136	0.22	0.50	1.88	1854	1863–2002	0.47	51
THT		133	0.18	−0.98	3.03	1839	1917–2005	0.45	48
IGI		216	0.16	−0.08	0.71	1722	1796–2004	0.42	45
DJT		174	0.18	−0.63	2.01	1635	1811–2005	0.43	46
TIG		226	0.20	−0.98	2.69	1742	1814–2000	0.44	47
LMO		156	0.15	−1.05	5.43	1871	1849–2001	0.37	42
RPN		155	0.16	−0.08	2.00	1832	1902–2004	0.41	44
THG		148	0.17	−0.25	0.80	1885	1902–1998	0.32	35
PIP		149	0.26	−0.15	0.89	1859	1898–2006	0.63	65
KES		95	0.23	0.11	0.54	1854	1916–2006	0.62	64
BNP		301	0.21	−0.31	2.28	1416	1772–2001	0.59	60
AEH		277	0.34	−0.08	0.89	1679	1774–2005	0.73	74
OUT		439	0.34	−0.15	0.92	1036	1602–1990	0.62	63
BOC		168	0.50	0.86	2.83	1756	1896–2006	0.79	80
DJE		126	0.47	0.30	0.42	1845	1899–2006	0.82	83
TOB		138	0.36	0.34	−0.01	1856	1887–2006	0.71	72
THN		112	0.31	0.70	1.77	1866	1894–2006	0.66	70
OUZ	Tunisia	137	0.27	0.53	0.20	1898	1928–2003	0.37	42
AID		166	0.24	0.69	0.95	1882	1899–2003	0.39	42
DHA		93	0.28	0.78	3.16	1905	1912–1998	0.52	57
SAD		137	0.46	0.33	0.13	1756	1909–1990	0.72	73
JEB		77	0.28	0.31	0.99	1902	1955–2001	0.60	62
OUD		111	0.34	0.46	0.35	1871	1917–2004	0.67	68

Statistics: [a] mean sample segment length, [b] standard deviation, [c] skewness, [d] Kurtosis, [e] the first year that the EPS (expressed population signal) is greater than 0.85 (Wigley et al. 1984), [f] mean correlation among radii, [g] explained variance in the first principal component of the series over the common interval

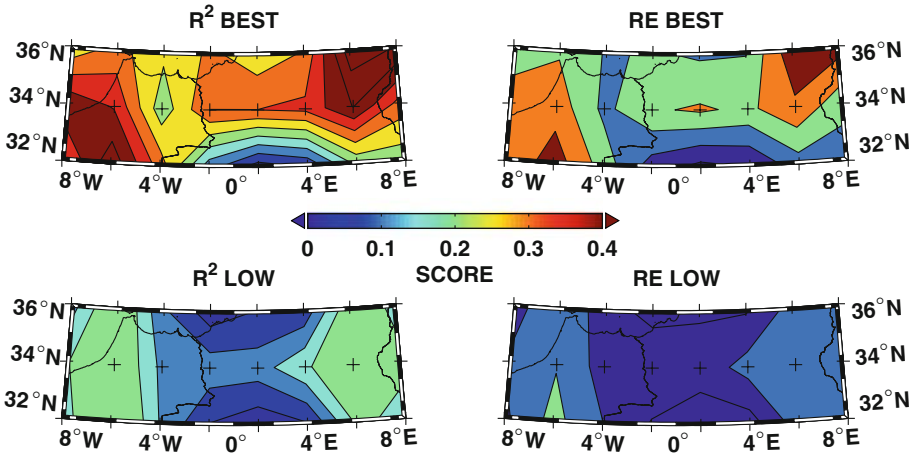

Fig. 4 Reconstruction skill maps for split sample cross validation using a late calibration period (1969–2003) and a early validation period (1931–1968). 'Best' R^2 and RE statistics are the highest values for this skill metric, in nearly all cases corresponding to the best replicated nest. 'Low' values are the scores for the nest with the least skill at each grid point, in most but not all cases corresponding to the nest with the fewest available chronology predictors

captured for well-replicated nests. Therefore, for regions with adequate tree-ring samples, these values are on par with those from the North American Drought Atlas (Cook et al. 2004, 2007). The reduction of error (RE) is consistently greater than zero in Morocco, regardless of the calibration/validation period considered. In eastern Algeria and Tunisia, however, RE approaches or falls below zero, particularly when using a late calibration period, although using the full reliable instrumental period results in an improved reconstruction of the mean and hence an improved RE score in the eastern region. We note that using the mean of all available tree ring chronologies for a given nest as a single predictor results in very similar reconstructions and spatiotemporal patterns of reconstruction (Touchan et al. 2008a). Using principal components (PCs) from the orthogonal decomposition of the tree ring series in each nest, however, is overall less skillful, particularly in the central portion of the domain, apparently because the predictor PCs in some cases isolate localized or species-specific variance as opposed to large-scale climate variability. For this reason we believe that the point-to-point regression approach to reconstruction used here, and successfully applied in North America (Cook et al. 2004), remains for the moment the best approach to climate field reconstruction for this region with our existing network.

In the middle and southern portion of the target domain, particularly in interior Algeria, the reconstruction resolves very little of the variance in the instrumental field, there is little to no skill in the reconstruction even for the most recent century, and the reconstructed grids do not span the full target time period (Figs. 4, 5, 6, Supplemental Materials). This is due to the paucity of tree ring chronologies within the search radius of these grid points (Figs. 1, 8). Limited or poor instrumental data over a portion of this region may also exacerbate the difficulty in developing skillful reconstructions of this portion of the field.

4.3 Spatiotemporal drought patterns

Based on these maps describing the spatial pattern of skillful reconstructions, we develop two regional mean time series to characterize the longitudinal poles of the field (Figs. 7, 8). The 'Western' includes the 4 grid points with consistently high R^2 and RE scores in the southwestern portion of the domain, while the 'Eastern' subregion includes three grid

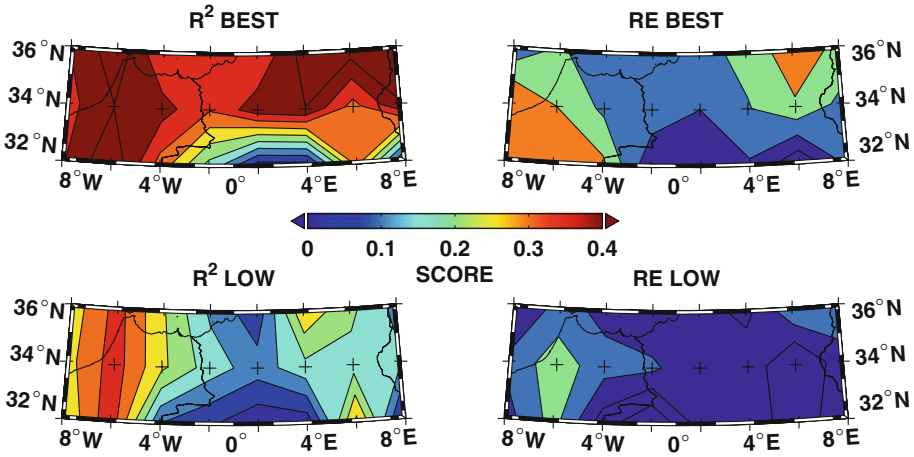

Fig. 5 Reconstruction skill maps for split sample cross validation using a early calibration period (1931–1968) and a late validation period (1969–2003). 'Best' R^2 and RE statistics are the highest values for this skill metric, in nearly all cases corresponding to the best replicated nest. 'Low' values are the scores for the nest with the least skill at each grid point, in most but not all cases corresponding to the nest with the fewest available chronology predictors

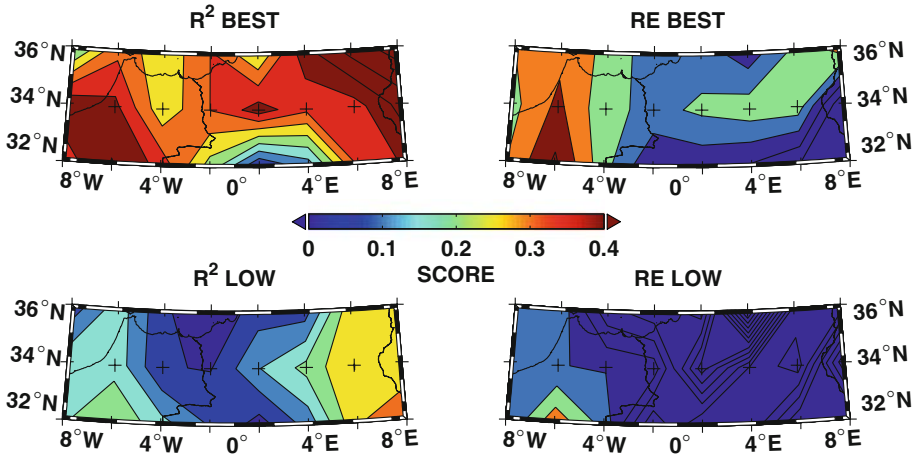

Fig. 6 Reconstruction skill maps for split sample cross validation using the full period for calibration period (1931–2003), with validation by a leave-one-out jackknife procedure. 'Best' R^2 and RE statistics are the highest values for this skill metric, in nearly all cases corresponding to the best replicated nest. 'Low' values are the scores for the nest with the least skill at each grid point, in most but not all cases corresponding to the nest with the fewest available chronology predictors

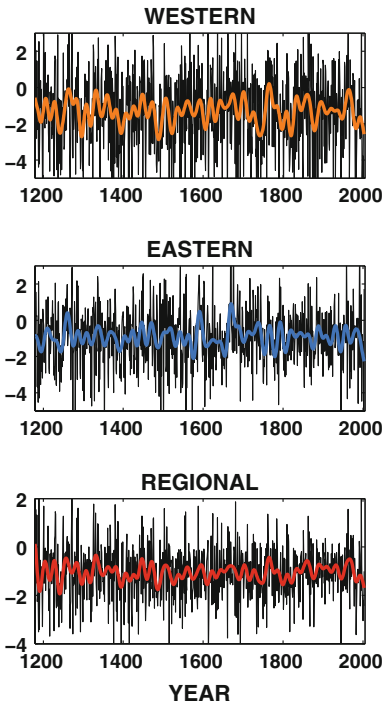

Fig. 7 Regional drought reconstructions from northwestern Africa. Western (*top*), eastern (*middle*), and regional mean (all 24 grid cells, *bottom*) annual and 20-year Butterworth lowpass filtered PDSI reconstructions. See text for definition of the Western and Eastern regions

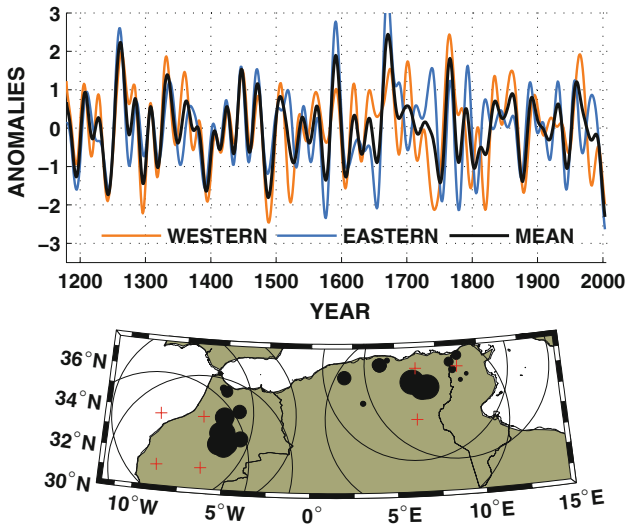

Fig. 8 Regional drought reconstructions from northwestern Africa. *Top panel* shows the 20-year low pass filtered standardized reconstructed PDSI from the western and eastern grid points and their mean (7 grid cell). Decadal-scale drought is widespread of the region when the regional time series are in phase, as they are through much of the early part of the record until 1500, the nineteenth century, and most recent decades. The *bottom panel* map shows the PDSI grid points (in *red*) of which the western and eastern mean time series are composed. Tree ring sites are shown by *filled circles* whose size scales with the length of the chronology. The 500 km radius range rings shown around each of the western and eastern grid points demonstrates that the eastern and western regional series are independent, with no predictors in common

points at the northwestern corner of the field that similarly show the most skill over the length of the reconstruction (Fig. 8). Correlation between the grid points that make up the western regional composite is high ($r = 0.89$ to $r = 0.99$, $n = 825$, $p < 0.001$), while the individual grid points from the eastern region show greater heterogeneity ($r = 0.25$ to $r = 0.68$, $n = 825$, $p < 0.001$). Reassuringly, this mirrors the instrumental record, where the western grid points show higher intercorrelation ($r = 0.57$ to $r = 0.89$, $n = 73$, $p < 0.001$) than the eastern grid points ($r = 0.13$ to $r = 0.85$, $n = 73$, $p < 0.26$ to $p < 0.001$).

In Morocco, the most severe multiyear droughts as reflected in the lows of 20-year smoothed reconstructed PDSI are observed in the mid-13th, late 13th, late 14th, late 15th, mid-18th and late 19th centuries, and in the most recent decade (Fig. 8, top). In the eastern part of the reconstructed field most severe droughts are in the late 12th, mid-13th, late 14th, late 16th, mid-17th, mid-18th, late 18th, early 19th, mid-20 centuries, and the most recent decade. A count of dry years in a moving 20-year window gives an alternative measure of drought history (Fig. 8). By

this measure, periods ending in the late 14th, mid-18th and mid-19th centuries are epochs of highest drought-frequency in Morocco (western region); and periods ending in the mid-thirteenth century dominate in the eastern region (Fig. 9). At the broader regional scale, however, the most recent decades of the twentieth century emerge as periods of highest drought frequency since perhaps the 13th and 16th centuries (bottom plots, Fig. 9).

Using our field reconstruction, we can also construct a 'Drought Area Index' (DAI) similar to that used by Cook et al. (2004), to characterize the spatial extent of droughts in time (Fig. 10). Our DAI calculation is based on the number of reconstructed grid cells with values below certain thresholds. Periods of spatially-extensive droughts tend to mirror periods of low mean regional PDSI (Fig. 10), and widespread droughts were most common between 1300 and 1500, the early nineteenth century, and the most recent decades. Recent drought therefore appears in the current reconstruction to also be notable for persistence in both extent and severity.

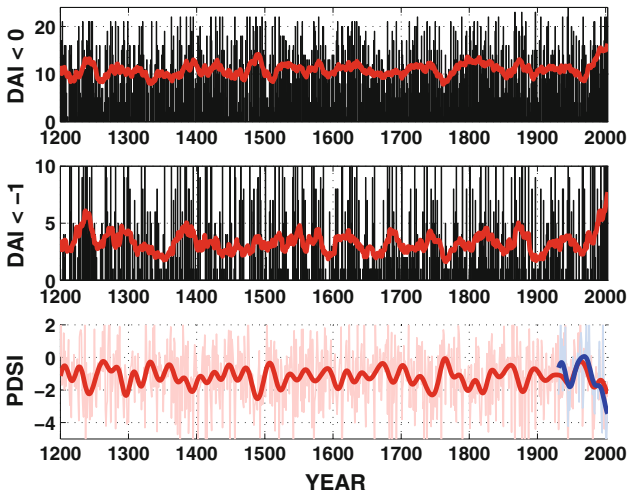

Fig. 10 Drought area index for northwestern Africa. Following Cook et al. (2004), we calculate the number of grid cells with PDSI values (**a**) less than 0, and (**b**) less than −1, in the full reconstructed field (24 grid cells) for each year. The mean western+eastern (7 grid cell) PDSI time series is shown by the *red line* in (**c**), with the instrumental data (Dai et al. 2004) for the same region and same months overlaid in *blue*. *Thick lines* are the 20 year Butterworth lowpass optimally filtered values (Mann 2004)

4.4 Drought frequency and coherence

Cross-spectral analysis of the full length of the reconstructed PDSI in the western and eastern parts of the study area is summarized in Fig. 11. Neither spectrum suggests significant overall periodicity, though both show a tendency for increased variance in a broad band centered near 7 years (Fig. 11a,b). The full-period coherency plot suggests weak coherence over perhaps half of the frequency axis, with a sharp jump in coherence at the same 7 year wavelength notable for high variance in both series. For no frequencies, however, does squared-coherency over the full period of the reconstruction exceed 0.30. The phase spectrum indicates west and east are largely in-phase. The weakly significant departure from zero-phase at wavelengths shorter than about 2.5 years can probably be disregarded, as the suggested phase-difference is less than the sampling interval of the data. The low squared coherency of east with west reflects their low simple correlation: (reconstruction, $r = 0.23$, $n = 825$, $p < 0.0001$; instrumental, $r = 0.36$, $n = 73$, $p < 0.0018$). The high statistical significance derives from the sample length rather than magnitude of correlation. The low correlation is not an artifact of averaging over gridpoints: no bivariate correlation between reconstructed gridpoint PDSI for a western and eastern gridpoint exceeds 0.22.

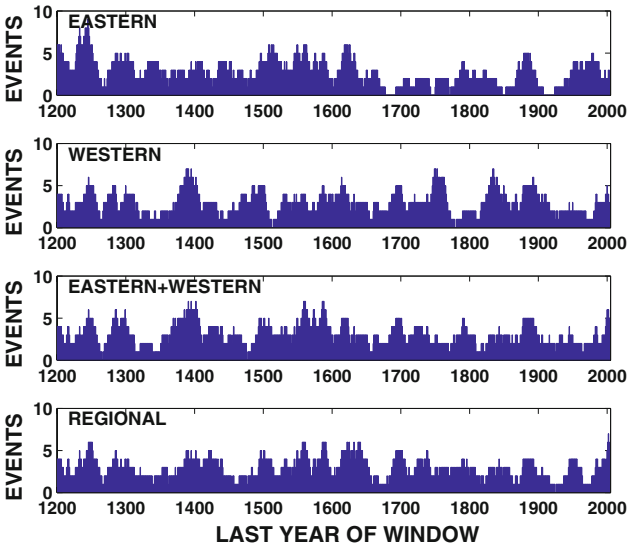

Fig. 9 Frequency of drought events in 20 year windows where the PDSI value for that year is less than or equal to one standard deviation below the long term reconstructed mean. Windowed event counts are shown for the eastern and western regions (*top 2 panels*), as defined in the text, as well as the average of both eastern and western (7 grid points) and the complete 24 grid point mean. The *bottom panel* therefore includes parts of the grid with minimal or no reconstruction skill, and therefore while it is perhaps more spatially representative of the entire region, it is less statistically reliable

The spectra of reconstructions is affected by many aspects of data processing, including and particularly standardization. Our use of residual chronologies for the PDSI reconstruction conditions the spectrum, as autoregressive (AR) pre-whitening would tend to shift the spectrum of a series generated by an autoregressive process toward the spectrum of white noise. The choice of residual chronologies over standard chronologies however was

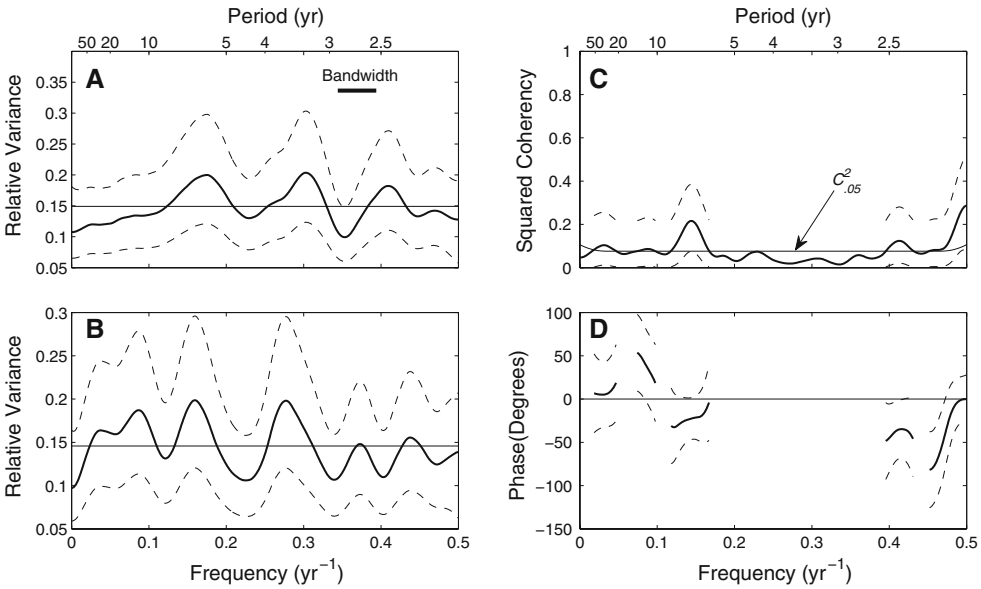

Fig. 11 Cross-spectral analysis of west-average and east-average reconstructed PDSI. Plotted are the spectrum of West (**a**); spectrum of East (**b**); squared-coherency of West with East (**c**); and phase of West with East (**d**). *Horizontal lines* on (**a**) and (**b**) are theoretical white-noise spectra. *Arrow* in (**c**) points to threshold squared coherency required for rejection of null hypothesis of zero coherency at $\alpha = 0.05$. *Dashed lines* are 95% confidence intervals. Following Bloomfield (2000), phase is ill-defined when squared coherency is not significantly different from zero

guided by a comparison of the autocorrelation properties of PDSI and standard chronologies in the region. Other studies have suggested more low-frequency variability (Esper et al. 2007). Future studies will explore the sensitivity of drought reconstructions in the region to standardization choices. A temporal and spectra comparison of our reconstruction with the Morocco PDSI time series reconstruction by Esper et al. (2007) is available in Supplemental Material (Figure S1, S2).

Wavelet coherence analysis allows phase and cross spectral relationships between east and west to be explored as a function of time. Figure 12 confirms a visual evaluation of Fig. 8 that drought variability in the two subregions is largely coherent and further emphasizes an in-phase relationship prior to A.D. 1500 at decadal to multidecadal frequencies. After that time, coherence is restricted to decadal, in-phase variability. Common power at multidecadal frequencies returns in the twentieth century, although it is briefly out of phase until both regions show trends toward drier conditions through the end of the time period covered by the chronologies. These observations hint at coherent, drier multidecadal intervals during the Medieval Climate Anomaly and the current anthropogenic warming, although the precise mechanisms that might cause this are at the moment unknown.

4.5 Association with broad-scale climate modes

4.5.1 North Atlantic oscillation

Correlations of the two regional reconstructions (western and eastern) with NAO index suggest variable influence across the region. The western series correlates negatively ($r = -0.33$, $N = 140$, $p < 0.0001$) with the NAO index over the common period 1864–2003. The eastern series is uncorrelated with NAO ($r = 0.06$, $N = 140$, $p = 0.45$) over the same period. The direction of the relationship (wet with negative NAO) for the western part of the grid is consistent with previous studies relating the NAO to cool-season precipitation in the Iberian Peninsula (Goodess and Jones 2002) and the western Mediterranean region (Glueck and Stockton 2001; Xoplaki et al. 2004; Knippertz et al. 2003a, b). Although our reconstruction variable (May-Aug PDSI) is not directly seasonally matched to the NAO window of

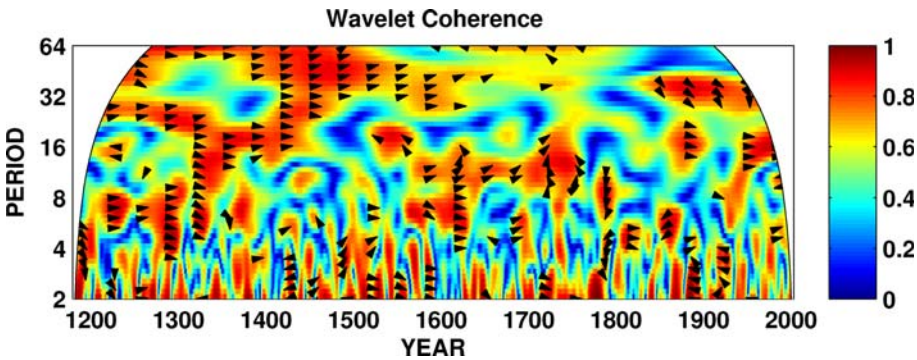

Fig. 12 Wavelet coherence (Maraun and Kurths 2004) between the western and eastern regional mean time series. Phase is indicated by *arrows* (shown here only when coherence exceeds 0.65), with *arrows* pointing to the right (0°) indicating in-phase variability. Only values not within the 'cone of influence' of end effects are shown

precipitation influence in the region, tree-growth in Morocco is apparently linked strongly enough to the NAO via the influence of winter precipitation on growing season soil moisture (c.f. Cook et al. 1999) for a signal to emerge in the Western reconstructed grid points.

Correlation of the western and eastern mean time series with winter (NDJFM) mean sea level pressure over Europe as reconstructed by Luterbacher et al. (2002), covering the period of their common overlap (1660–1999), also supports this analysis (Fig. 13). Significant ($p < 0.001$) negative correlations between the western PDSI time series and winter SLP are observed over the study region, particularly Morocco, indicating that higher pressure over northwestern Africa has been associated with Moroccan drought over the last 340 years. The eastern drought time series, however, has insignificant although positive correlations that are focused over Europe.

4.5.2 *Sea surface temperatures*

Simple field correlations between the western and eastern mean drought reconstructions and winter (DJF) Kaplan sea surface temperature anomalies (SSTA, 1857–2003), show overall negative but weak associations between global SSTA and drought in northwestern Africa (Fig. 14). That is, dry conditions in our study region occasionally coincide with warmer than normal ocean temperatures. Overall, drought in Morocco is weakly correlated with El Niño events and a warm Indian Ocean, while drought in Algeria and Tunisia is more associated with warm tropical Atlantic SSTs and the Atlantic tripole. Correlation coefficients here are also relatively weak. Li et al. (2003) previously investigated the influence of the Atlantic SST tripole on Morocco and western Algerian precipitation, finding that the response of north African rainfall to Atlantic SST influences was both nonlinear and seasonally dependent. They found that in both models and observations a positive SST tripole in early and mid winter causes reduced rainfall (Li et al. 2003). The Indian Ocean pattern is consistent with some climate model studies (Hoerling and Kumar 2003). Esper et al. (2007) also posited a teleconnection between Moroccan drought and Pacific SST, although their hypothetical relationship is the opposite as detected here by simple correlations, if limited direct proxy knowledge about Medieval Pacific SSTs (e.g. Cobb et al. 2003; Seager et al. 2007b) is correct; however, such a relationship could very well be frequency-dependent or be a function of the large-scale mean state of the ocean-atmosphere system.

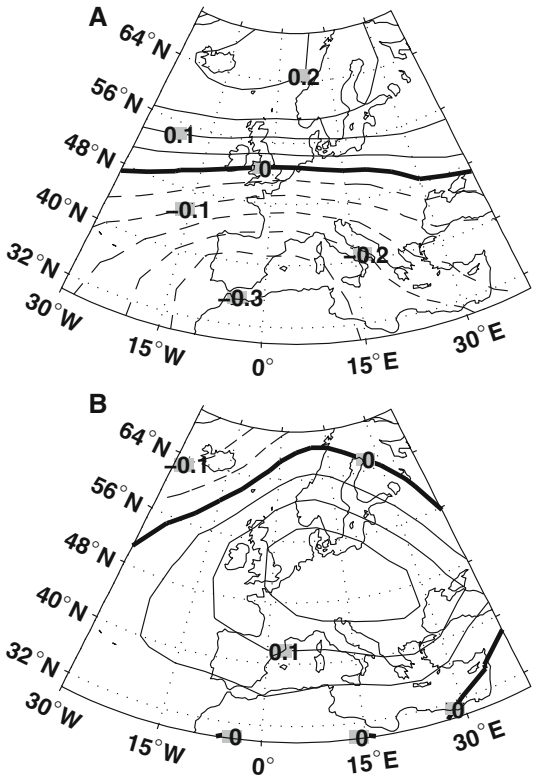

Fig. 13 Long-term association between reconstructed drought and sea level pressure. Field correlation between the (**a**) western and (**b**) eastern PDSI time series and the SLP reconstruction by Luterbacher et al. (2002) over the period 1660–1999. Negative values are indicated by *dashed lines* and the zero line is in *bold*

However, the difficulty in interpreting regional drought patterns in terms of broad-scale SST forcing is illustrated in Fig. 15. Examining two significant but spatially distinct droughts during the twentieth century, one with a west-to-east drought/pluvial dipole (1981 and 1982) and the other a homogeneous drought signal over the region (1945 and 1946), reveals two different SST configurations. The heterogenous spatial PDSI pattern in the summers of 1981 and 1982 was associated with an overall warmer Pacific, Indian and tropical Atlantic Ocean, with colder SSTs in the northwestern Pacific and extratropical north Atlantic. In contrast, during the region-wide drought of 1945–1946, the eastern Pacific experienced generally colder, La Niña conditions, as well as a colder Indian and warmer north Pacific Ocean, and an anomalously warm North Atlantic (although see Thompson et al. (2008)). In terms of remote Pacific Ocean forcing of regional drought, the severe and widespread postwar drought is therefore at odds with both the inference from simple correlations (Fig. 14) as well as the SST anomaly pattern that have been associated with the drought that began in 1998 (Hoerling and Kumar 2003). Collectively, this suggests that broad-scale SST forcing can only explain a portion of PDSI variability in our study region and that the causes of particular spatiotemporal drought fingerprints are complex, a finding in agreement with our earlier analyses (Touchan et al. 2008a).

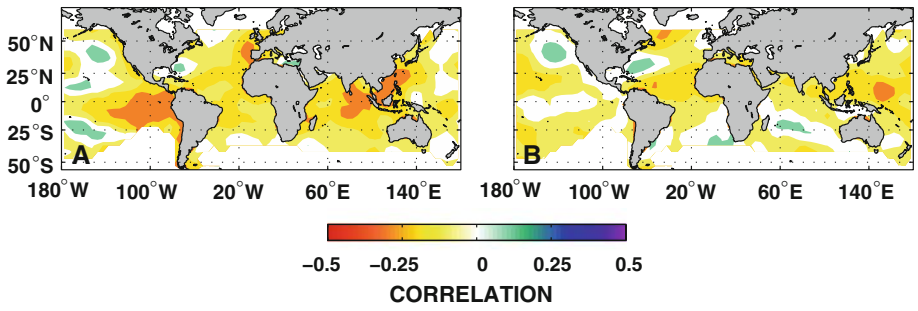

Fig. 14 Association between drought reconstructions and sea surface temperature. Spatial correlations between (**a**) Western (Morocco) and (**b**) Eastern (Algeria and Tunisia) PDSI time series and winter (DJF) Kaplan sea surface temperature anomalies (Kaplan et al. 1998) over their common period, 1856–2003

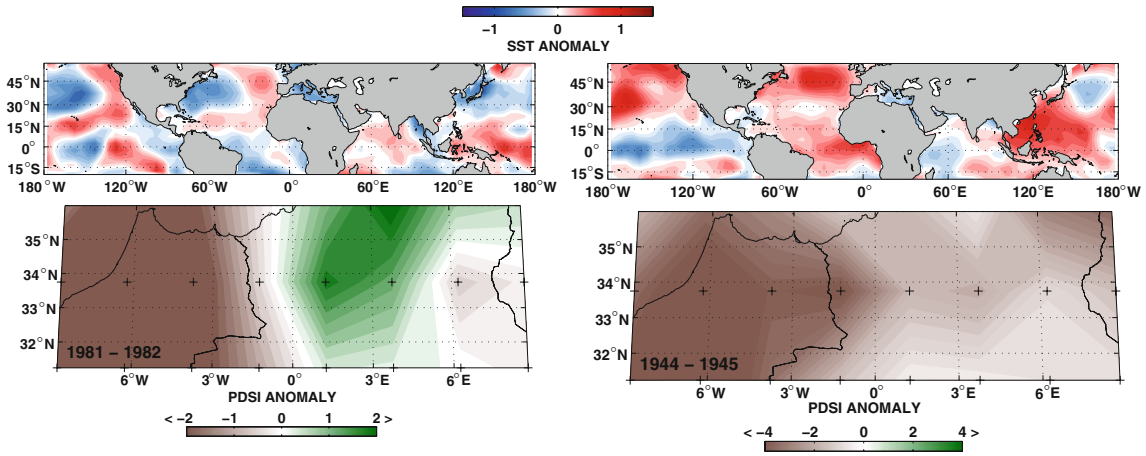

Fig. 15 Examples of paired drought and SST anomalies from northwestern Africa. Mean winter (DJF) SST anomalies (Kaplan et al. 1998) and following summer (MJJA) reconstructed PDSI anomalies for 1981 and 1982 (*left column*) and 1944 and 1945 (*right column*) for historical droughts in our study region. The PDSI anomalies are calculated by removing the long-term, full reconstruction mean from each grid point, in order to compensate for non-zero baselines in the Dai et al. (2004) data set

4.6 General circulation models simulations

Our hypothesis is that twentieth century drought in northwestern Africa reflects a combination of natural variability and radiatively forced trends (Held and Soden 2006; Seager et al. 2007a). A comparison of our regional mean reconstruction to forced and control climate model scenarios supports this (Fig. 16), and our hypothesis cannot be rejected based on these data. The mean of the 68 '20c3m' ensemble members declines throughout the last 150 years, indicating progressive drying of northwestern Africa. In contrast, even the mean of the preindustrial control simulations shows decadal variability but no long-term trend. Our reconstruction likely does therefore represent a combination of natural and anthropogenic variability, with a recent decline in drought index values consistent with the forced model simulations, but variability in the earlier part of the century that is indistinguishable from the control simulation. Caution here is warranted since models, gridded instrumental data, and our reconstructed field all show large interannual variability, and the models have virtually no agreement at the shortest time scales. Moreover, it is not yet possible to unequivocally distinguish between substantial unforced decadal variability and an apparent trend at the end of the reconstructed time series. Nevertheless the dominant low-frequency feature of forced models and actual PDSI is the tendency toward dry conditions into the early twenty-first century.

5 Summary and conclusions

We present a new climate field reconstruction of drought in Morocco, Algeria, and Tunisia back to A.D. 1179, incorporating the largest number of tree-ring chronologies yet available from the region into a spatially continuous grid. This reconstruction now provides long-term climatological, ecological, archaeological, and historical context for recent drought in the region. Our point-to-point method allows us to identify the southern and central portion of the target field as clear priorities for future tree-ring sampling in the region. Based on temporal (Figs. 7, 8), spatial (Fig. 10), and spectral (Figs. 11, 12) analysis, our reconstruction demonstrates that when considered at the regional scale, the latter half of the twentieth century is one of the driest in the last nine centuries. There are significant uncertainties,

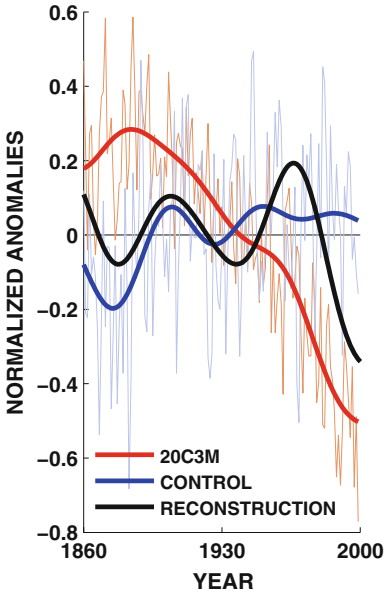

Fig. 16 CMIP3 modeled and tree-ring reconstructed changes in drought severity in northwestern Africa over the last century. The results of the twentieth century ('*20c3m*') forced simulation (*red*) are the ensemble mean of 68 simulations from 23 models. The mean of the last 150 years of the preindustrial control simulation is the ensemble average of 26 simulations from 20 models. *Heavy lines* show 20 year low pass Butterworth filtered values (Mann 2004). Our reconstructed values represent a mix of natural and apparently forced drought variability over the region, with both twentieth century forced simulations and reconstructed values showing an evident decline toward dry conditions during the last several decades. Reconstruction and simulations are normalized and shown as anomalies from their twentieth century mean

both from sparse site coverage of drought-sensitive chronologies in some areas and from a declining number of tree-ring chronologies available back in time (see Supplemental Material). Our analysis has accordingly focused on broad and well-validated spatial features (e.g. eastern vs western) of reconstructed drought variability. A finer-scale climatological interpretation, including inferences on past seasonal atmospheric circulation anomalies over the region, the role of broad-scale sea surface temperature forcing, and the specific combination of factors which result in distinct regional spatiotemporal drought fingerprints, should eventually be possible as the network of tree-ring sites is expanded in space and time.

Our findings from the current network of sites are consistent with a robust projection from general circulation models (Fig. 16) that anthropogenic greenhouse gas emissions will result in the imminent drying of subtropical regions. While interpretation of trends approaching the endpoints of time series with substantial unforced low-frequency variability requires the utmost caution, our conclusions are thus far consistent with one of the more robust features of general circulation model projections of the future (Held and Soden 2006; Seager et al. 2007a). A long-term trend toward more arid conditions in northwestern Africa may of course be punctuated by occasional wet anomalies, but governments and natural resources managers in the region need to be prepared forthwith to deal with future drying.

Acknowledgments In Morocco we thank the Ministry of Agriculture, the Department of Forestry, and the National School of Forest Engineering, the Director (Driss Misbah) and the staff of Direction of the Rif High Commissariat of Water, Forestry and Combating Desertification, the Director (Abdelaziz Houseini) and the staff of Direction of the Oriental High Commissariat for Water, Forestry and Combating Desertification, the Director (Mustapha Khalladi) and the staff of Direction of Moyen Atlas of High Commissariat of Water, Forestry and Desertification Combating, the Chief (Mohamed Benziane) and staff of the National Center of Forestry Research, and the Director and staff of the National School of Forest Engineering for making this study possible. We wish to thank our colleagues from Algeria, especially Abdelmalek Mohamed Azzedine Idder (Ecosystem Laboratory, University of Ouargla), Belkitir Dadamoussa (former Director, Ecosystem Laboratory, University of Ouargla), Titah (General Director of Forests), Mohamed Seghir Mellouhi (former General Director of Forests), Hocine Medjedoub (former Director of Forest, Betna), Abdallatif Guasmi (Director of Forest, Batna), Saidi Belkacem (Directory of Forest in Khenchela), Haddad Moussa (National Park of Tikdjda, Bouira), Mohamed Tizioui, Said Abderahmani (National Park of Belezma), Athmane Briki (Betna Forest Department), Ali Loukkas (National Park of Theniet el had), Chabane Cheriet (Director of Forest in Tiziouzou), Tidjani Mohamed El-khamis (former President of the University of Ouargla), and Ahmed Boutarfaia (President of the University of Ouargla). We wish to thank our colleagues from Tunisia, including Toumi Lamjed (Directeur général de l'ISPT (Institut Sylvo-Pastoral de Tabarka), Mougou Abdelaziz Président de l'IRESA (Institution de la Recherche et l'Enseignement Supérieur Agricole), Rejeb Néjib Directeur général de l'INRGREF (Institut national de recherche en génie rural, eaux et forêts), Fekih Salem Ahmed Ridha Directeur génŕal des forê ts, and the forest technicians of Siliana, Kef, Kasserine, Ain Draham, and Jendouba for their great help and support in making this study possible. We thank Rachid Ilmen, Mohamed El Youssfi, and Rachid Azzam, Salaheddine Saadine, and Said Slimani for their valuable field assistance. We thank Christopher Baisan, Gregg Garfin, Jeffrey Dean, Paul Sheppard, and Martin Munro for their advice and suggestions. We also thank Jeffrey Balmat, Nesat Erkan, Jim Burns, Jeremy Goral, Julie Wong, and Salah Eddine Sadine for their valuable assistance in both the field and laboratory. We acknowledge the modeling groups, the Program for Climate Model Diagnosis and Intercomparison (PCMDI) and the WCRP's Working Group on Coupled Modelling (WGCM), for their roles in making available the WCRP CMIP3 multi-model dataset. Support of that dataset is provided by the Office of Science, U.S. Department of Energy. This is LDEO Contribution 7342 (KJA). Funding was provided by the US National Science Foundation, Earth System History (ESH0317288).

References

Aloui A (1982) Recherches dendroclimatologiques en Kroumirie (Tunisie). PhD thesis, Universite Aix-Marseille III

Aloui A, Serre-Bachet F (1987) Analyse dendroclimatologique comparée de six populations de chêne zeen et d'une population

de pin maritime du nord-ouest de la Tunisie. Ecol Mediterr 13(3):55–74
Ammann CM, Wahl ER (2007) The importance of the geophysical context in statistical evaluations of climate reconstruction procedures. Clim Change 85(1–2):71–88. doi:10.1007/s10584-007-9276-x
Belkheiri A, Compte JP, Khabotti AE, Lahmouri A, Mirouah D (1987) Bilan de cinq anées de sécheresse au Maroc. Rev Eau Dev 3:10–26
Berger A, Guiot J, Mathieu L, Munaut A (1979) Cedar tree-rings and climate in Morocco. Tree-Ring Bull 39:61–75
Bloomfield P (2000) Fourier analysis of time series: an introduction. Wiley-Interscience. New York
Brooks K, Ffolliott PF, Gregersen HM, Thames JL (1991) Hydrology and the management of watersheds. Iowa State University Press, Ames
Chbouki N (1992) Spatio-temporal characteristics of drought as inferred from tree-ring data in Morocco. PhD thesis, University of Arizona, Tucson
Chbouki N, Stockton CW, Myers D (1995) Spatio-temporal patterns of drought in Morocco. Int J Climatol 15:187–205
Chou C, Neelin JD, Chen CA, Tu JY (2009) Evaluating the "rich-get-richer" mechanism in tropical precipitation change under global warming. J Clim 22(8):1982–2005
Cobb KM, Charles CD, Cheng H, Edwards RL (2003) El Ninõ-Southern Oscillation and tropical Pacific climate during the last millennium. Nature 424:271–276
Cook ER (1985) A time series approach to tree-ring standardization. PhD thesis, University of Arizona, Tucson, AZ, USA
Cook ER, Briffa KR (1990) A comparison of some tree-ring standardization methods. In: Cook ER, Kairiukstis LA (eds) Methods of dendrochronology. Kluwer, Dordrecht, pp 104–123
Cook ER, Briffa KR, Jones PD (1994) Spatial regression methods in dendroclimatology—a review and comparison of 2 techniques. Int J Climatol 14:379–402
Cook ER, Meko DM, Stahle DW, Cleaveland MK (1999) Drought reconstructions for the continental United States. J Clim 12(4):1145–1162
Cook ER, D'Arrigo RD, Mann ME (2002) A well-verified, multiproxy reconstruction of the winter North Atlantic oscillation index since AD 1400. J Clim 15:1754–1764
Cook ER, Woodhouse CA, Eakin CM, Meko DM, Stahle D (2004) Long-term aridity changes in the western United States. Science 306(5698):1015–1018
Cook ER, Seager R, Cane MA, Stahle DW (2007) North American drought: reconstructions, causes, and consequences. Earth Sci Rev 81(1–2):93–134
Critchfield HJ (1983) General climatology, 4th edn. Prentice-Hall, Englewood Cliffs, 453 pp
Dai A, Trenberth KE, Qian T (2004) A global dataset of Palmer drought severity index for 1870–2002: relationship with soil moisture and effects of surface warming. J Hydrometeorol 5(6):1117–1130
Esper J, Frank D, Büntgen U, Verstege A, Luterbacher J, Xoplaki E (2007) Long-term drought severity variations in Morocco. Geophys Res Lett 34:L17702. doi:10.1029/2007GL030844
Glueck MF, Stockton CW (2001) Reconstruction of the North Atlantic oscillation, 1429–1983. Int J Climatol 21:1453–1465
Goodess CM, Jones PD (2002) Links between circulation and changes in the characteristics of Iberian rainfall. Int J Climatol 22:1593–1615
Held IM, Soden BJ (2006) Robust responses of the hydrological cycle to global warming. J Clim 19(21):5686–5699
Hoerling MP, Kumar A (2003) The perfect ocean for drought. Science 299:691–694
Holmes R (1983) Computer assisted quality control in tree-ring dating and measurement. Tree-Ring Bull 44:69–75
Kaplan A, Cane MA, Kushnir Y, Clement AC, Blumenthal MB, Rajagopalan B (1998) Analyses of global sea surface temperature 1856–1991. J Geophys Res 103(C9):18,567–18,589
Kempes CP, Myers OB, Breshears DD, Ebersole JJ (2007) Comparing response of *Pinus edulis* tree-ring growth to five alternate moisture indices using historic meteorological data. J Arid Environ. doi:10.1016/j.jaridenv.2007.07.009
Knippertz P, Christoph M, Speth P (2003a) Long-term precipitation variability in Morocco and the link to the large-scale circulation in recent and future climates. Meteorol Atmos Phys 83(1):67–88
Knippertz P, Ulbrich U, Marques F, Corte-Real J (2003b) Decadal changes in the link between El Nino and springtime north Atlantic oscillation and European-north African rainfall. Int J Climatol 23:1293–1311
Lamb PJ, Hamly ME, Portis DH (1997) North Atlantic oscillation. Geo Observateur 7:103–113
Li S, Robinson WA, Peng S (2003) Influence of the North Atlantic SST tripole on northwest African rainfall. J Geophys Res 108(D19):4594–4610
Luterbacher J, Xoplaki E, Dietrich D, Rickli R, Jacobeit J, Beck C, Gyalistras D, Schmutz C, Wanner H (2002) Reconstruction of sea level pressure fields over the Eastern North Atlantic and Europe back to 1500. Clim Dyn 18:545–561
Mann ME (2004) On smoothing potentially non-stationary climate time series. Geophys Res Lett 31(7):L07214. doi:10.1029/2004GL019569
Maraun D, Kurths J (2004) Cross wavelet analysis: significance testing and pitfalls. Nonlinear Process Geophys 11(4):505–514
Meehl GA, Covey C, Delworth T, Latif M, McAvaney B, Mitchell JFB, Stouffer RJ, Taylor KE (2007) The WCRP CMIP3 multimodel dataset. Bull Am Meteorol Soc 88:1383–1394
Meko D (1997) Dendroclimatic reconstruction with time varying predictor subsets of tree indices. J Clim 10:687–696
Meko DM, Woodhouse CA (2005) Tree-ring footprint of joint hydrologic drought in Sacramento and Upper Colorado river basins, western USA. J Hydrol 308(1–4):196–213
Messaoudene M (1989) Approche dendroclimatologique et productivité de Quercus afares Pomel et Quercus canariensis Willd. dans les massifs forestiers de l'Akfadou et de Beni-Ghobri en Algérie. PhD thesis, Université Aix-Marseille III
Messaoudene M, Tessier L (1997) Relations cerne-climat dans des peuplements de Quercus afares Willd et Quercus canariensis Pomel en Algérie. Annales des Sciences forestiéres 54:347–358
Munaut AV, Berger AL, Guiot J, Mathieu L (1979) Dendroclimatological studies on Cedars in Morocco. In: Gautier D, Lesgards R, Aubry M (eds) Evolution of planetary atmospheres and climatology of the Earth, pp 373–379
Nicholson SE, Wigley TML (1984) Drought in Morocco. Part I: the general climatology of drought. Report to the Conseil Supérieur de l'eau, Maroc
Palmer WC (1965) Meteorological drought. Technical report, U.S. Weather Bureau Research Paper 45
Safar W, Serre-Bachet F, Tessier L (1992) Les plus vieux pins d'Alep vivants connus. Dendrochronologia 10:41–52
Seager R, Ting M, Held I, Kushnir Y, Lu J, Vecchi G, Huang HP, Harnik N, Leetmaa A, Lau NC, Li C, Velez J, Naik N (2007a) Model projections of an imminent transition to a more arid climate in southwestern North America. Science 316(5828):1181–1184
Seager R, Graham N, Herweijer C, Gordon AL, Kushnir Y, Cook ER (2007b) Blueprints for Medieval hydroclimate. Quat Sci Rev 26:2322–2336
Serre-Bachet F (1969) Variations de l'epaisseur des anneux chez le Thuya de Barbarie (*Tetraclinis articulata* (Vahl) Mast.) et climat en Tunisie. Annales de la Faculte des Sciences de Marseille 42:193–204

Stokes M, Smiley T (1968) An introduction to tree-ring dating. University of Chicago Press, Chicago

Swearingen WD (1992) Drought hazard in Morocco. Geogr Rev 82(4):401–412

Swetnam TW (1985) Using dendrochronology to measure radial growth of defoliated trees. USDA Forest Service, Cooperative State Research Service, Agriculture Handbook 639:1–39

Tessier L, Nola P, Serre-Bachet F (1994) Deciduous Quercus in the Mediterranean region: tree-ring/climate relationships. New Phytol 126:355–367

Thompson DWJ, Kennedy JJ, Wallace JM, Jones PD (2008) A large discontinuity in the mid-twentieth century in observed global-mean surface temperature. Nature 453(7195):646–649

Till C (1987) The summary response function of *Cedrus atlantica* in Morocco. Tree-Ring Bull 47:23–36

Till C, Guiot J (1990) Reconstruction of precipitation in Morocco since 1100 AD based on *Cedrus atlantica* tree-ring widths. Quat Res 33:337–351

Touchan R, Anchukaitis KJ, Meko DM, Attalah S, Baisan C, Aloui A (2008a) Long term context for recent drought in northwestern Africa. Geophys Res Lett 35(13):L13,705

Touchan R, Meko DM, Aloui A (2008b) Precipitation reconstruction for northwestern Tunisia from tree rings. J Arid Environ 72(1887–1896)

Trewartha GT (1981) The Earth's problem climates, 2nd edn. The University of Wisconsin Press, Madison, 371 pp

Wigley TML, Briffa KR, Jones PD (1984) On the average value of correlated time series, with applications in dendroclimatology and hydrometeorology. J Clim Appl Meteorol 23:201–213

Wilson R, Tudhope A, Brohan P, Briffa KR, Osborn TJ, Tett S (2006) Two-hundred-fifty years of reconstructed and modeled tropical temperatures. J Geophys Res 111:10,007

Xoplaki E, Gonzalez-Rouco JF, Luterbacher J, Wanner H (2004) Wet season Mediterranean precipitation variability: influence of large-scale dynamics and trends. Clim Dyn 23:63–78